Development and preclinical evaluation of equine-derived hyperimmune serum against SARS-CoV-2 infection in K-18 hACE2 transgenic (Tg) mice

E.A. Onen[1], E.K. Demirci[2]

[1] Kocak Pharmaceutical Company, Biotechnology and Vaccine R&D, Tekirdag, Turkey
[2] Histology and Embryology Department, Istanbul Faculty of Medicine,
Istanbul University, Istanbul, Turkey

Correspondence to: E.A. Onen, e-mail: alponen@gmail.com, tel.: +90 530 863 79 34

Abstract

This study aimed to develop an equine-derived hyperimmune serum against SARS-CoV-2 and evaluate its efficacy as a potential immunotherapy tool for the treatment of known and potential variants of COVID-19 in preclinical trials.

The novelty of this study is the whole virus and ALUM gel adjuvant formula. The horses were immunized using a whole inactivated SARS-CoV-2 antigen, and the final purified hyperimmune serum showed high plaque reduction neutralization ($PRNT_{50}$) neutralizing titers. The efficacy of the hyperimmune serum was evaluated histopathologically and biochemically in the lungs, hearts, and serum of K18 hACE2 transgenic mice (n=45), which is an accepted model organism for SARS-CoV-2 studies and was challenged with live SARS-CoV-2.

Serum treatment improved the general condition, resulting in lower levels of proinflammatory cytokines in the blood plasma, as well as reduced viral RNA titers in the lungs and hearts. Additionally, it reduced oxidative stress significantly and lessened the severity of interstitial pneumonia in the lungs when compared to infected positive controls.

The study concluded that equine-derived anti-SARS-CoV-2 antibodies could be used for COVID-19 prevention and treatment, especially in the early stages of the disease and in combination with antiviral drugs and vaccines. This treatment will benefit special patient populations such as immunocompromised individuals, as specific antibodies against SARS-CoV-2 can neutralize the virus before it enters host cells. The rapid and cost-effective production of the serum allows for its availability during the acute phase of the disease, making it a critical intervention in preventing the spread of the disease and saving lives in new variants where a vaccine is not yet developed.

Keywords: COVID-19, cytokines, equine-derived hyperimmune serum, heart, histology, K18 hACE2 mice, lung, SARS-CoV-2

Introduction

Severe acute respiratory syndrome coronavirus-2 (SARS-CoV-2) is a novel virus from the Coronaviridae family that can cause severe viral pneumonia and multisystemic symptoms. These symptoms include severe headaches, gastrointestinal symptoms, rhinitis, neurological and olfactory disorders. Approximately 5% of patients infected with SARS-COV-2 experience severe illness or die (Winkler et al. 2020).

Studies on treatments for COVID-19 have focused mainly on antiviral drugs such as remdesivir, ASC09, lopinavir/ritonavir, arbidol, interferon-alpha, and thymosin alpha-1. The use of these drugs in COVID-19 treatment is still being investigated and further research is ongoing to determine their effectiveness and safety (Zhang et al. 2020, De Vito et al. 2023, Li et al. 2023).

Recent studies have also shown that monoclonal antibodies can provide effective treatment for COVID-19. These antibodies are designed to target specific parts of the SARS-CoV-2 virus and can be produced in large quantities through biotechnology. They are currently being used as a treatment option for people who are at high risk of severe illness or hospitalization due to COVID-19, but their large-scale production is hard and costly (Moreira-Soto et al. 2021).

Several hyperimmune serum formulations have been created from horses' plasma that was immunized with S1 protein, inactivated SARS-CoV-2 whole virus, or recombinant proteins (S1, N, and SEM) of the virus. These hyperimmune serum have demonstrated high neutralizing antibody levels in vitro in many global studies (Luis Eduardo Cunha et al. 2020, Pan et al. 2020, León et al. 2021, Botosso et al. 2022, Li et al. 2023). Equine hyperimmune serum is a well-known and easily scalable technology for producing high titers of neutralizing antibodies against specific pathogens such as rabies, tetanus, diphtheria and MERS-CoV (Moreira-Soto et al. 2021, Li et al. 2023). The specific antibodies against SARS-CoV-2 can neutralize the virus before it enters the host cells (Pan et al. 2020, Botosso et al. 2022).

This study aimed to examine the efficacy of a newly developed and cost-effective equine hyperimmune serum formulation on K18 hACE2 mice, which are model organisms used to study SARS-CoV-2. The use of hyperimmune serum formulations, created from horses' plasma vaccinated with an aluminium hydroxide gel mixture of inactivated SARS-CoV-2, has shown high in vitro neutralization capacity. We used histopathological methods to assess the morphological changes in the nasal passages, lungs, and hearts, and measured virus titers in the lungs and hearts, as well as proinflammatory cytokine levels in the serum and oxidative stress in the lungs. These findings highlight the potential of equine hyperimmune serum as a treatment option for COVID-19.

Materials and Methods

Inactivated SARS-CoV-2 antigen preparation

Virus seed lots were generated from a SARS-CoV-2 strain (Vial no.31242/12.05.2020) isolated from bronchoalveolar lavage specimens or throat swabs from a hospitalized patient in the early days of the COVID-19 outbreaks by the Turkish Ministry of Health. SARS-CoV-2 was propagated and produced in VERO CCL-81 cell line (ATCC, USA), inactivated with β-propiolactone (Sigma, USA), purified by multimodal chromatography and adsorbed by ALUM adjuvant (Engin Alp Onen et al. 2022). Antigen quantity in the final bulk was adjusted to 5.1×10^6 TCID$_{50}$ SARS-CoV-2 inactivated viral antigen /animal/dose (Fig. 1A).

Animal immunization for horse hyperimmune serum production

Before the study, all animals were subjected to prophylactic vaccination and deworming programs that are routinely utilized at the KODEHAL farm (Tekirdag/TURKEY).

To produce polyvalent hyperimmune serum, four healthy horses (3 males and 1 female), aged 3-5 years and weighing approximately 350-450 kg each, were used. Each horse was immunized subcutaneously four times at 7-day intervals (on days 0, 7, 14, and 21) in various positions of the dorsal region.

All horses were monitored daily for food and water intake, clinical conditions, and behaviors. Blood samples were collected every 7 days just before the next inoculation, and 14 days after the last inoculation (up to day forty-eight since the first inoculation).

Horse plasma collection

Serum samples were collected using an automated plasmapheresis system called Haemonetics PCS2® (Boston, USA), and serum neutralizing antibody levels were evaluated on day 0, 28, 36, and 48 after the first dose of antigen (Fig. 1B). Plasma was collected for therapeutic apheresis procedures.

Production of a bench-scale equine F(ab')2 fraction

We pooled plasma from all animals to initiate the F(ab')2 production process. In a reactor, we added 3 L of injection water and 15 L of 90% phenol solution to 2 L of plasma. To digest and eliminate the Fc portion,
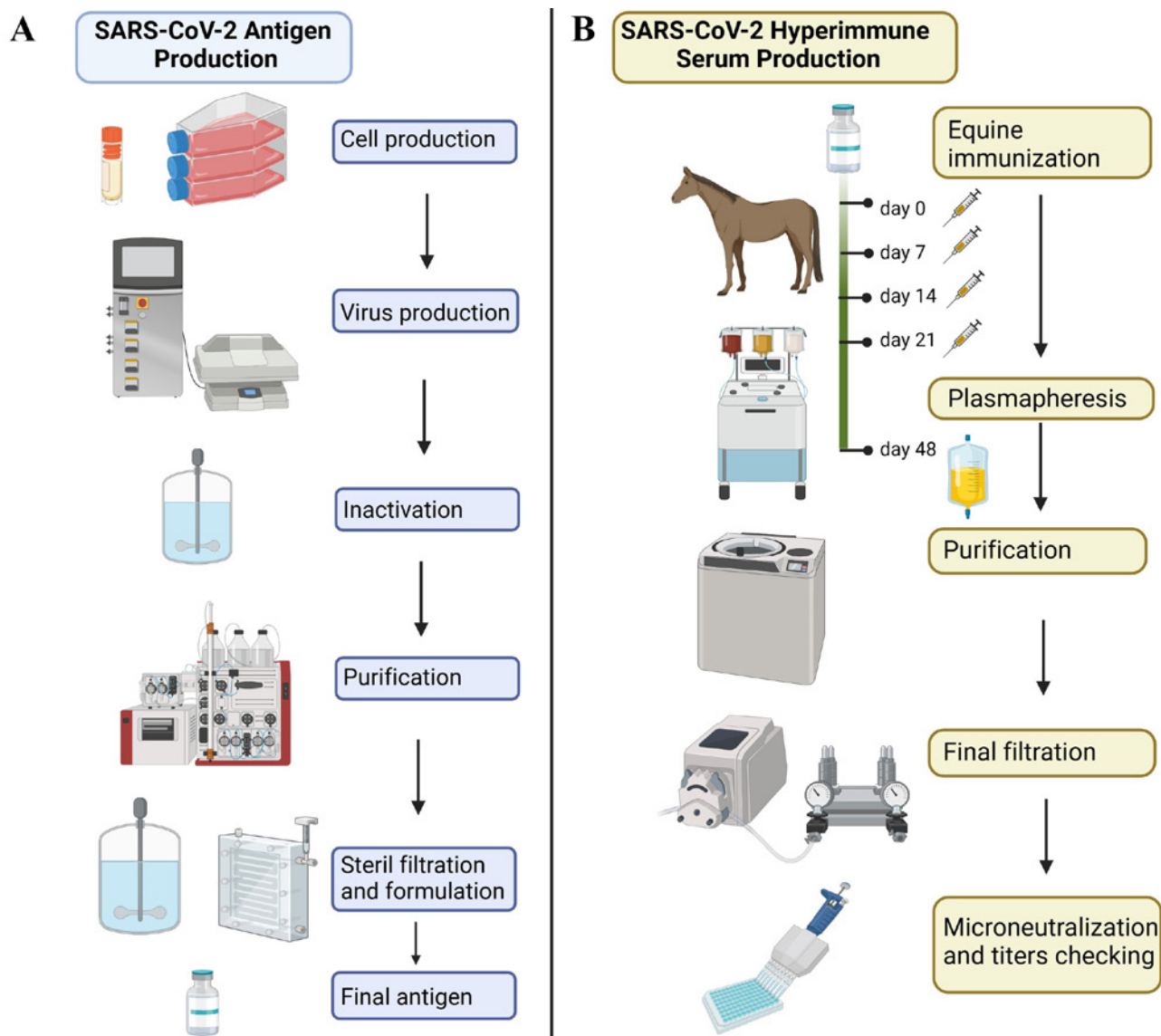
Fig. 1. Antigen preparation and equine-derived hyperimmune serum production against to SARS-CoV-2 flow chart. (Illustration was created with BioRender.com)

we added 1.25 g/L of pepsin (Sigma Aldrich, USA) under agitation, adjusted the pH to 3.2 with HCl, and kept the sample under agitation for 10 minutes. We then stirred the sample at 37°C and adjusted the pH to 4.2 with sodium hydroxide. We added sodium pyrophosphate decahydrate (12.6 mM) and toluene (10 μM) under constant agitation. Subsequently, we added ammonium sulphate at 12% (m/v) and incubated the solution at 55°C for 1 hour. To separate the F(ab')2 fragments, we precipitated the Fc portion and subsequently filtered it under pressure at constant agitation, recovering the F(ab')2 from the liquid phase.

To precipitate F(ab')2 from the liquid phase, we added ammonium sulphate at 19% (m/v) and performed a second precipitation under constant agitation and alkaline pH. Subsequently, we diafiltered the solution using a 30 kDa tangential ultrafiltration system until ammonium sulphate became undetectable in the retentate. We then buffer-exchanged the samples with 15 mM NaCl and added 90% phenol solution to a final concentration of 0.3% (v/v). After sterile filtration with a 0.2 μm PES filter, we stored the F(ab′)2 product at 4°C (Fig.1B).

Plaque reduction neutralization antibody test

We assessed whether equine serum could neutralize SARS-CoV-2 in vitro by collecting serum on day 0 and every week after three booster immunizations on days 28, 36, and 48 following the initial immunization. The collected serum samples were then diluted with two-fold Eagle's Modified Essential Medium (EMEM) and mixed with 100 $TCID_{50}$ live virus. The mixture of serum and virus was added to confluent Vero
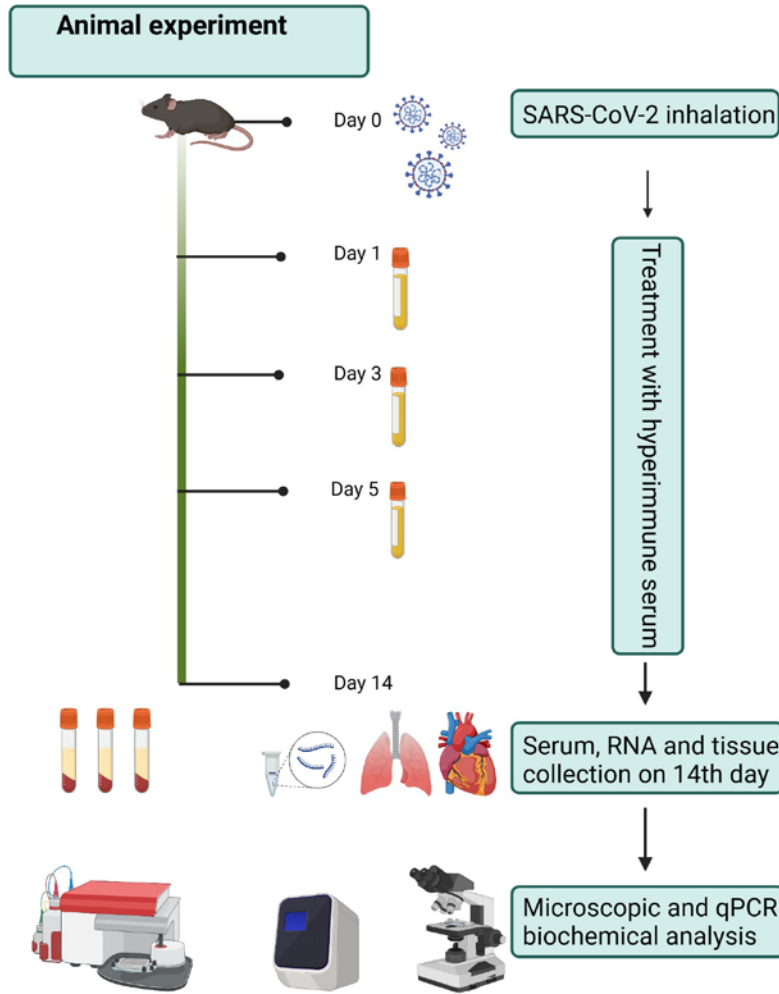
Fig. 2. Animal experiment scheme. Design and execution of experiments, which includes administering treatments and collecting data. (Illustration was created with BioRender.com)

CCL-81 cells in 24-well plates. After the 1 h incubation, the inoculums were removed and then covered with 0.4% agarose MEM (Minimum Essential Media). After the plates were incubated for 3-4 days at 37°C, they were fixed with 10% formaldehyde, and stained with (0.4-1% v/v) crystal violet in methanol. PRNT endpoint titers were expressed as the reciprocal of the last serum dilution. The PRNT titer was calculated based on a 50% reduction in plaque count ($PRNT_{50}$).

Animal experimentation

Forty-five adult K18 hACE2 male and female mice, 8-9 weeks-old, were separated into four groups. The study included a control group of 10 animals. Another group of 10 animals were infected with SARS-CoV-2, while a separate group of 10 animals received treatment with equine hyperimmune serum only. Additionally, 15 animals were infected with SARS-CoV-2 and received equine hyperimmune serum treatment, administered three times with a one-day interval between each administration.

On day 0, mice in SARS-CoV-2 and SARS-CoV-2 + equine hyperimmune serum groups were challenged with 5×10^4 live viruses/50 µl by the intranasal route. On the first day post-infection (dpi), mice in Equine hyperimmune serum and SARS-CoV-2+equine hyperimmune serum group (n=15) were injected intraperitoneally with equine hyperimmune serum (2500 $PRNT_{50}$/0.2 ml).

At 3- and 5-days post-infection, mice were given another dose of purified equine hyperimmune serum. Ten mice were left as negative controls without any treatment, and 10 mice were left as positive controls infected by SARS-CoV-2 but not given any treatment.

Weight changes and general health status of male mice from each group were recorded individually on a daily basis for a period of 14 days. Animals that did not survive for fourteen days underwent necropsy. On the 14th day, we performed dissection after decapitation under ketamine and xylazine anesthesia in accordance with ethical rules and collected tissue samples from each animal (Schoell et al. 2009). The tissue sam-

ples obtained for biochemical analyses, including blood, lung, and heart, were stored at -80°C, while samples for histological analyses of the respiratory system organs and heart were fixed in a fixative solution (Fig. 2).

Quantitative real time RT PCR to detect viral load in lung and heart tissues.

Lung and heart samples were collected from each group of mice and homogenized using 2 mm glass beads in TissueLyser II equipment (Qiagen, Germany) at 30-35 Hz for 2-3 min twice, followed by centrifugation at 13,000 rpm (Eppendorf 5804R centrifuge) for 40 s. All viral nucleic acids were extracted from lung and heart homogenates of mice using the

RNA isolation kit (High Pure RNA Tissue Kit, ROCHE, Germany) according to the manufacturer's instructions. A commercial one-step 2X RT-PCR Master Mix (Genesig® *Primer* design, USA) and a commercial quantitative COVID-19 Real Time RT-PCR kit (Primer design 2019-nCoV Genesig® Advanced Kit, USA) were used for the polymerase chain reaction. The primers and probe in commercial kit target the RdRp (RNA dependant RNA polymerase) gene locus of the SARS Coronavirus. We performed amplification in 96-well non-transparent plates on a LightCycler 480 Real-Time PCR instrument (ROCHE, Germany). Each 20 μL reaction mix includes 10 μL 2X Master Mix, 2 μL 5 μmol/L probes, 20 μmol/L forward and reverse primer mix, 5 μL nuclease-free water, and 5 μL nucleic acid extract. Real-time PCR conditions set up 10 min at 55°C for reverse transcription (RT) reaction, 2 min at 95°C for Taq polymerase enzyme activation, and 40 cycles of 3 s at 95°C and 30 s at 55°C in the polymerase chain reaction. Viral load (copy number/μl) is calculated depending on the standard curve.

Dissection, tissue processing for light microscopy

After collecting blood samples, we removed the scalp and dissected it to access the sinus cavities and upper respiratory system. The thorax was then opened through the sternum, and the lungs and hearts were removed. Each tissue sample was fixed in neutral buffered formalin (pH: 7) for 24 hours.

To decalcify the bone tissues of upper airways, we used the formic acid-sodium citrate decalcification method (Suvarna et al. 2018). The decalcification process was monitored daily.

All the tissues and decalcified upper mice heads underwent routine paraffin tissue processing. We completed the embedding process according to the section surface, and we prepared a minimum of two paraffin blocks from each tissue. The tissue samples were sec-

tioned at a thickness of 4 μm using a Leica RM22555 Rotary Microtome.

Histochemical staining and evaluation

After deparaffinization, sections were passed through decreasing alcohol series and rinsed in distilled water.

For lung, heart and sinuses, we used hematoxylin-eosin for histopathological evaluation and applied Masson-Trichrome staining for various connective tissue changes expected to occur in the lung.

Two investigators unaware of the study groups examined staining pattern, differentiation of cells and surrounding tissues, morphological structure, inflammation and damage under a Leica DMLB light microscope.

The sinuses and olfactory epithelium were evaluated according to literature (Yu et al. 2022, Xu et al. 2020). Lungs and hearts were scored semi-quantitatively for inflammatory infiltrates as negative (-), mild focally positive (+), moderately positive (++) and strongly positive (+++) (Maccio et al. 2021). An additional scoring for the number of affected animals is also provided, and the different observed pathologies for the alveolar area, bronchi, and nasal cavity areas are scored as follows: For the alveolar area: The sum of animals with lymphocyte-dominant leukocyte infiltration in the interstitium, alveolar collapse, thickening of the alveolar septum, edema, and erythrocytes, as well as leukocyte infiltration around vessels. For the bronchi: The sum of animals exhibiting bronchial epithelial damage and congestion in the peribronchial vessels. For the nasal cavity: The sum of animals exhibiting squamous, olfactory, and respiratory epithelial damage.

Biochemical tests

Serum samples of transgenic mice are evaluated for oxidative stress parameters MDA, MPO, and GSH (Cat no. 40324, 40593, and 40371; Elabscience) with colorimetric assays according to manufacturer's instructions.

To evaluate inflammation, IL-1B, IL-6, IL-10, TNFα, and MCP-1 values were assessed with Multiplex Inflammation Panel Flow Cytometry Assay (MMX774, Antigenix, USA) according to manufacturer's instructions. Analyte concentrations of the sample are determined by comparison to known concentrations of a standard curve.

Statistical analyses

The data were analyzed using GraphPad Prism 9.4.0 (GraphPad Software, San Diego, CA, USA). Normality was tested using Shapiro-Wilk test. ANOVA
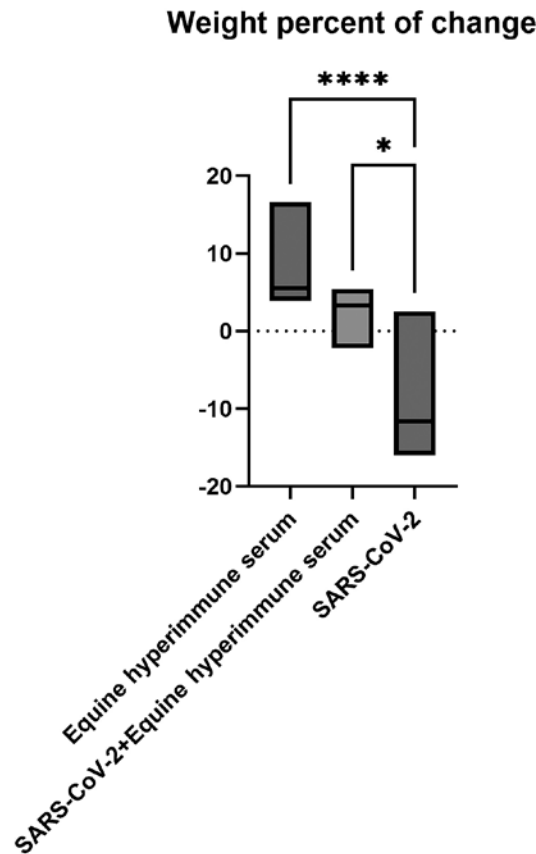
Weight percent of change

Fig. 3. The investigation aimed to evaluate the impact of SARS-CoV-2 infection. Significant differences were observed in weight percent change between the mouse groups.

and post-hoc Tukey test were used for normally distributed variables, while Kruskal-Wallis and post-hoc Dunn's test were used for non-normally distributed variables. Significance level was set at $p < 0.05$. Results are reported as mean $\pm$ SEM or median as appropriate.

Results

Daily weight changes and animal health status results

Beginning at 1 dpi with live SARS-CoV-2 virus at a concentration of 5×10^4 TCID50, mice underwent rapid weight loss, with the most significant loss occurring at 6 and 7 dpi. Within the initial 4-to-7-day period, more than half of the mice exhibited clinical symptoms and died. The surviving mice displayed clinical symptoms for the entire 14-day observation window, but these symptoms started to resolve by 10 to 12 dpi.

The group that received the hyperimmune serum showed less severe initial clinical symptoms compared to the untreated SARS-CoV-2 infected group. These symptoms included loss of grooming behavior, weight loss, and decreased responsiveness to the environment. The weight percent change showed significant diffe-

rences between groups with pairwise comparisons as follows: SARS-CoV-2 vs. SARS-CoV-2 + equine hyperimmune and SARS-CoV-2 vs. equine hyperimmune (Fig. 3).

Viral load quantification from tissue samples

According to this study, animals that died four days after virus infection had a high viral load in their lungs, as detected by quantitative RT-PCR. Although the viral load detected in the heart is lower than that in the lungs. The viral RNA load in the lungs and heart of the SARS-CoV-2 infected group treated with equine hyperimmune serum was significantly lower than that of the group infected with SARS-CoV-2 alone (Fig. 4).

Detection of equine-derived SARS-CoV-2 hyperimmune serum neutralization titers by Plaque Reduction Neutralization Antibody Test (PRNT$_{50}$)

Over time, the PRNT$_{50}$ titers for all four horses showed an increase, with an average PRNT$_{50}$ titer of 1:40,960 (Table 1).
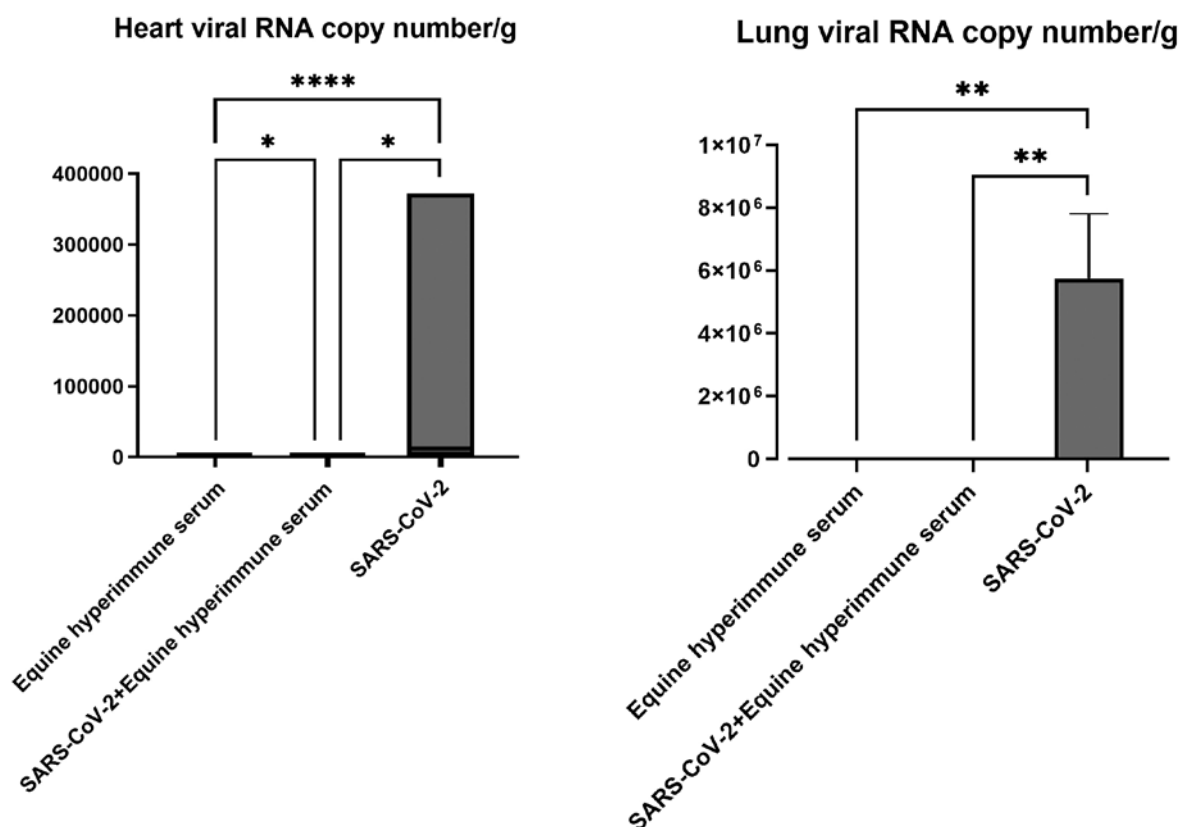
Fig. 4. There were significant differences in quantifying (RNA copy number/g) viral load observed in the lungs and hearts of the mouse groups (* p<0.05, ** p<0.01, *** p<0.001, **** p<0.0001).

Table 1. The equine hyperimmune serum $PRNT_{50}$ levels on various days after immunization with inactive SARS-CoV-2 antigen.

Equine-derived hyperimmune serum			
Date of sampling	Antigen Doses	$PRNT_{50}$	MEAN + SD
0. day	No priming	<16 <16 <16 <16	<16 $\pm$ 0
28. day	Prime + 1 booster dose	8192 4096 8192 8192	7168 $\pm$ 2048
36. day	Prime + 2 booster doses	16384 16384 8192 8192	12288 $\pm$ 4730
48. day	Prime + 3 booster doses	32768 32768 65536 65536	40960 $\pm$ 18918

Histopathological evaluation

The nasal passages of the groups treated with equine hyperimmune serum displayed similar morphology to the control group. However, in mice infected with SARS-CoV-2, the olfactory epithelium showed severe damage, with focal irregularities and necrosis. Inflammatory cells were found to infiltrate the lamina propria in that area. Some mice showed mild accumulation of mucus in their nasal passages. The squamous epithelium was not affected. The basal cells and nuclear layer of olfactory cells showed shrinkage of nuclei, indica-

Table 3. Semi-quantitative inflammatory scoring of hearts and lungs of K18-hACE2 transgenic mice infected with SARS-CoV-2 and treated with horse serum.

	Control	Equine hyperimmune serum	SARS-CoV-2 + Equine hyperimmune serum	SARS-CoV-2
Hearts	-	+	++	+++
Lungs	-	-	+	+++

-, no visible changes; +, mild focal or multifocal changes; ++, moderate multifocal changes; +++, moderate diffuse changes; ++++, severe diffuse changes

Table 4. The table displays the number of animals with the described pathologies in the specified areas (n=10 for each mouse group).

	Control	Equine HS	SARS-CoV-2+ Equine HS	SARS-CoV-2
Alveolar area				
Lymphocyte dominant leukocyte infiltration in the interstitium	0	0	7	9
Alveolar collapse	0	0	1	5
Thickening of alveolar septum	0	3	3	9
Edema and erythrocytes	1	1	3	8
Leukocyte infiltration around vessels	0	3	3	6
Bronchi				
Bronchial epithelial damage	0	0	3	7
Congestion in the peribronchial vessels	1	2	2	7
Nasal cavity				
squamous epithelium damage	0	0	0	0
olfactory epithelium damage	0	0	2	5
respiratory epithelium damage	1	1	3	6

ting the presence of apoptotic cells, and a few macrophages were present in the mucosal and submucosal areas. Inflammation was moderate in the SARS-CoV-2 infected group, while the SARS-CoV-2 infected equine hyperimmune serum treated group showed mild inflammation and mild epithelial lesions (Table 2).

The control and equine hyperimmune serum groups exhibited normal lung morphology. In the SARS-CoV-2 group, interstitial pneumonia of varying degrees and patchy areas of occluded airspaces was prominent. Lymphocyte-dominant mononuclear leukocyte infiltration in the interstitium, alveolar collapse, and thickening of the alveolar septum were visible. Some bronchioles were also affected, and some of the peribronchiolar vessels were congested. In some animals, edema and erythrocytes near the infected areas were observed, although this was rare (Table 3). The SARS-CoV-2 + equine hyperimmune serum group showed mild infection near bronchioles. The bronchiolar epithelium and alveolar morphology remained mostly preserved. Some small vessels had edema and congestion, and leukocyte infiltration of neutrophils, lymphocytes, and macrophages could be seen near these areas. Patchy areas of infiltration were rare and very small. Higher magnifications revealed a more pronounced difference in inflammatory cell infiltration and bronchiolar epithelial damage between the SARS-CoV-2 infection with and without equine hyperimmune serum treatment. (Fig. 5).

In comparing damage scores between groups, significant differences were observed in the alveolar area (p<0.0001) and bronchi (p=0.0054). Pairwise comparisons revealed distinctions between the equine hyperimmune-serum therapy + SARS-CoV-2 and SARS-CoV-2 groups (alveolar area p=0.0065, bronchi p=0.0021). However, no significant difference was found in the nasal cavity across groups (p=0.1617) (Table 4 and Fig. 6).

The control and serum groups had normal heart morphology. However, in the group infected with SARS-CoV-2, there was prominent small vessel endotheliosis, with most of the adventitia of small vessels showing mononuclear inflammatory cell infiltration (Fig. 7). Some blood vessels exhibited congestion. The infected areas had scattered degenerative myofiber changes, and some myocytes experienced necrosis due to virus application. Single cell eosinophilia without nuclear blurring indicated hypoxia and organelle degeneration. Myocardial fibers were wavy in some severely infected animals, which is a sign of myocardial
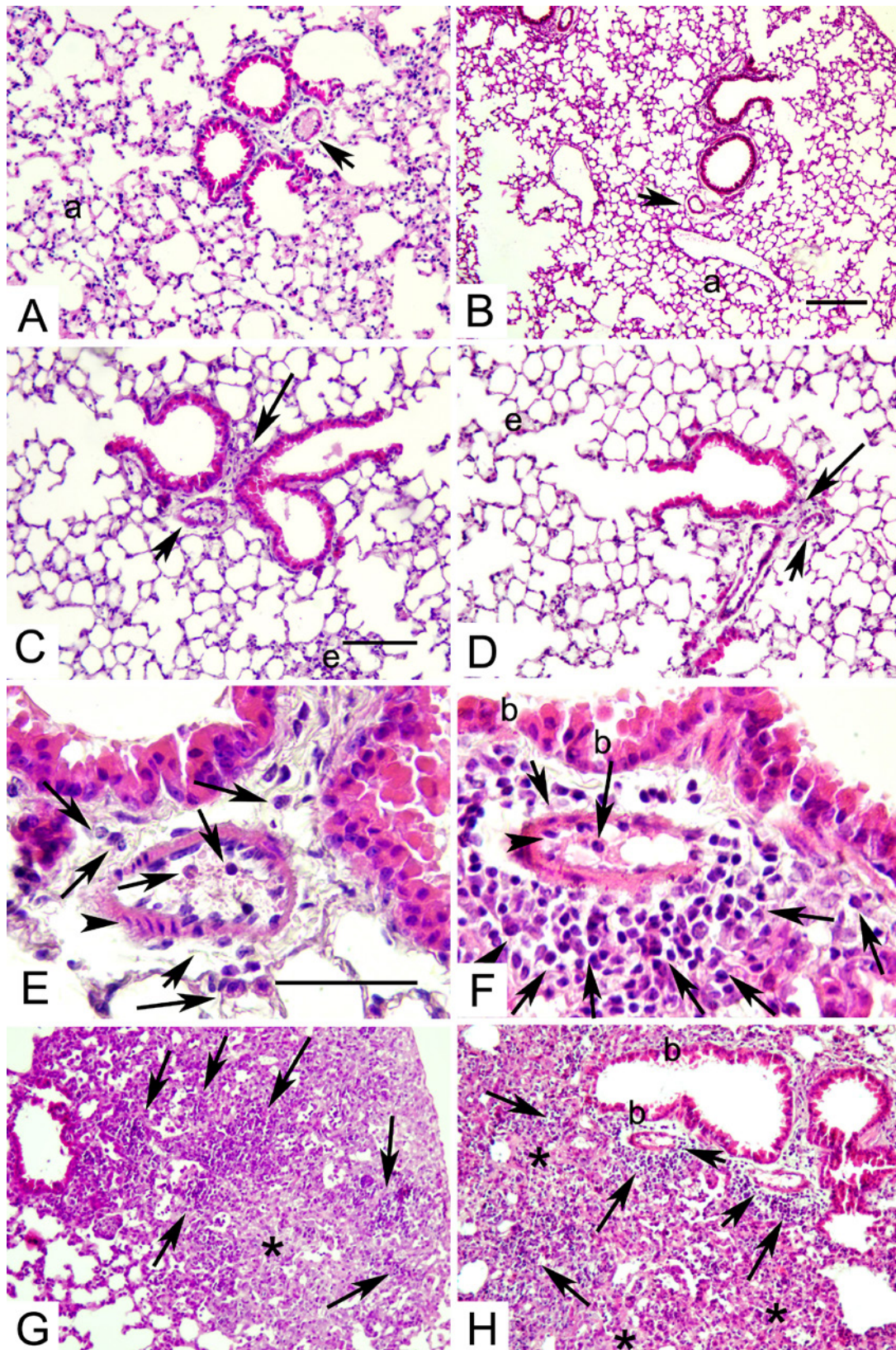
Fig. 5. The lungs of K18-hACE2 Tg mice: Control (A), equine hyperimmune serum-treated (B), SARS-CoV-2 + equine hyperimmu-
ne serum-treated (C, D, E), and SARS-CoV-2 groups (F, G, H). Indications show normal alveoli with thin alveolar septa (a),
blood vessels (short arrow), edema in alveolar airspaces (e), inflammatory cell infiltration (long arrow), bronchiolar epithelial
damage (b), and interstitial pneumonia with patchy areas of occluded airspaces (*). Hematoxylin and eosin staining was used.
A, C, D, G, and H were observed at x10 magnification, B at x4 magnification, and E and F (both are selected areas of C and H)
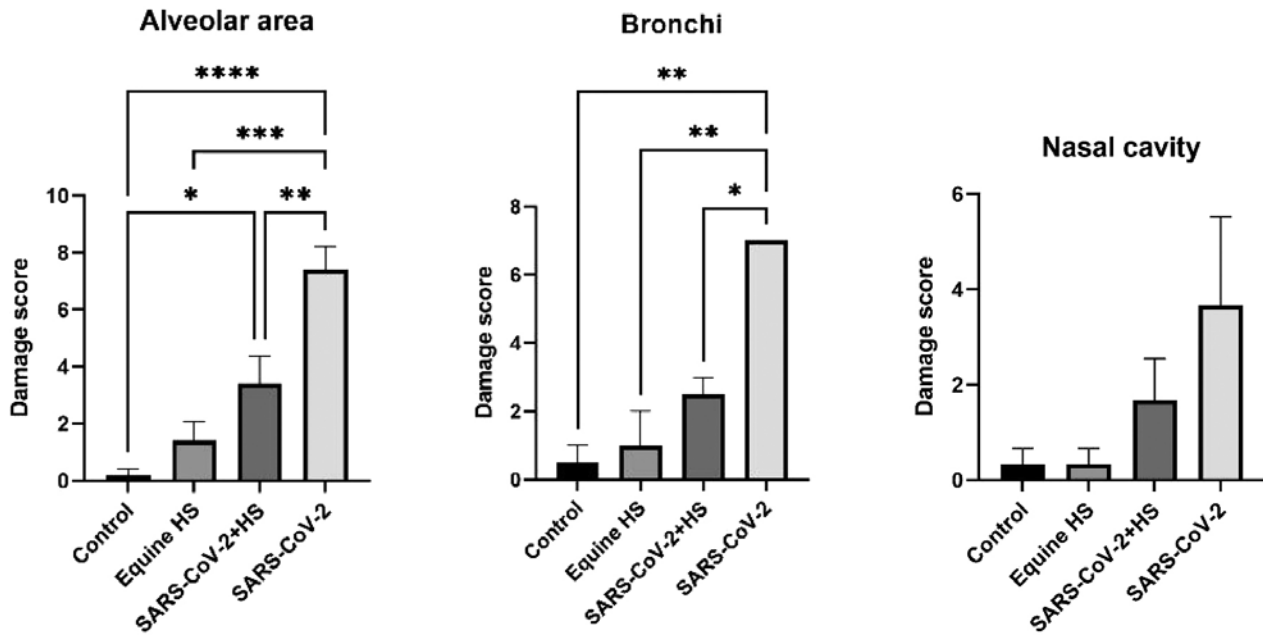at x40 magnification. The scale bars for x4, x10, and x40 represent 50 μm, 100 μm, and 200 μm, respectively.

Fig. 6. The panel presents the damage scores as mean ± SEM for each mouse group, along with statistical significances of pairwise comparisons, denoted as: * p<0.05, ** p<0.001, *** p<0.0001, and **** p<00001.

ischemia. Large coronary arteries had mild inflammatory cell infiltration in their adventitia. Intraventricular blood presented a large population of inflammatory cells. The endocardium, subendocardium, and myocardium were similarly affected. Cardiac pathologies were milder in the equine hyperimmune serum-treated infected group, with features like slightly swollen endothelium and a few eosinophilic-stained heart muscle cells. More than half of the vessels showed no inflammation, and most of the parenchyma was preserved (Fig. 7).

Biochemical tests

Proinflammatory cytokines, such as IL-6, IL-1β, TNF-α, IL-10, and chemokines MCP-1, showed strong increases in serum on 4-14 dpi only in SARS-CoV-2 inhaled control mice. However, cytokine levels that indicate inflammation and immunological disease remained significantly lower in the hyperimmune serum-treated group compared to the SARS-CoV-2 group.

As a measure of lipid peroxidation, levels of tissue MDA increase, while the level of the antioxidant GSH decreases. In this study, it has been observed that the increase in the levels of MDA recovers with equine derived hyperimmune serum treated group of mice. These results indicate that the hyperimmune serum treatment reduces oxidative stress and enhances the ability of cells to fight against free radicals. MPO is an enzyme that serves as a biomarker for inflammation. Similarly, the increased levels of MPO in the SARS-CoV-2 group imply that the virus could trigger

a more pronounced inflammatory response in the heart and lungs, as opposed to the treatment group (Fig. 8).

Discussion

During the early stages of a pandemic, when specific treatments were not yet available, passive immunotherapies using convalescent human plasma or animal-derived hyperimmune globulins were often the initial antiviral interventions. Previous research has explored the use of horse immunization to generate hyperimmune globulins against various viruses, including SARS-CoV, MERS-CoV, Ebola, and avian influenza, with varying levels of effectiveness against different variants of SARS-CoV-2. Pan et al. 2020 study suggested that F(ab')2 fragments from equine hyperimmune serum may have the ability to prevent COVID-19. In a study, Moreira-Soto et al. (2021), demonstrated varying levels of effectiveness of hyperimmune serum against variant strains in in-vitro neutralization tests of important SARS-CoV-2 variants. In addition, these F(ab')2 fragments bind to multiple epitopes of the SARS-CoV-2 RBD (receptor binding domain), suggesting that they can neutralize a broad spectrum of SARS-related coronaviruses and its variants (Pan et al. 2020).

The results of our study showed that SARS-CoV-2 infection in K18 hACE2 transgenic mice led to rapid weight loss and high mortality rates, consistent with previous research (Dong et al. 2022, Jha et al. 2022). The mice exhibited weight loss patterns similar to severe COVID-19 cases in humans reaching maximum weight
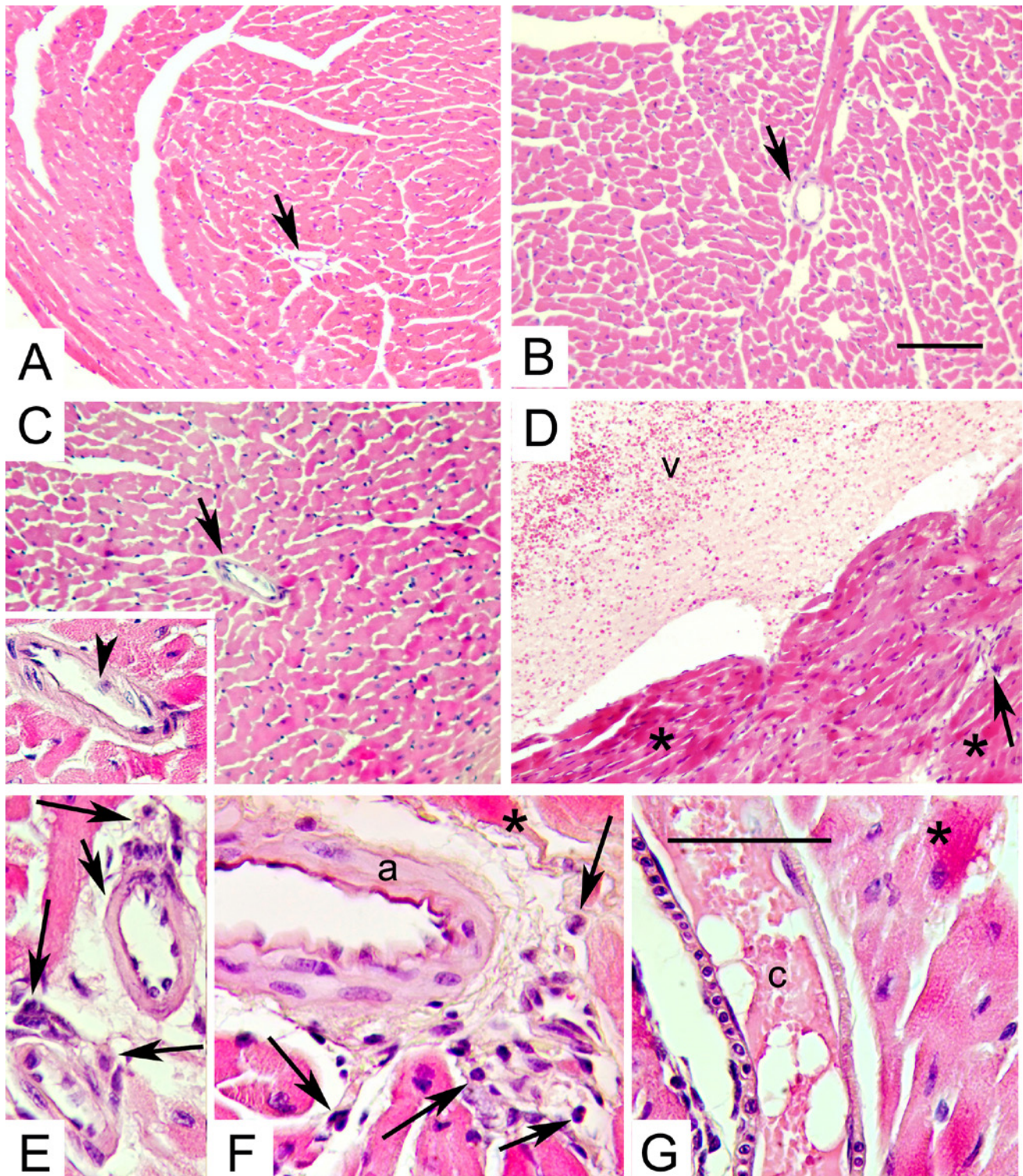
Fig. 7. Hearts from K18-hACE2 Tg mice: Control (A), equine hyperimmune serum-treated (B), SARS-CoV-2 + equine hyperimmune serum-treated (C, C inlet), and SARS-CoV-2 groups (D, E, F, G). Indications show blood vessels (short arrow), swollen endothelium (arrowhead), ventricle (v), eosinophilic-stained heart muscle cells (asterisk), inflammatory cells (long arrow), coronary artery (a), and congestion (c). Hematoxylin and eosin staining was used. A, B, C, and D were magnified at x10, while C inlet, E, F, and G were magnified at x40. The scale bars denote 50 µm and 100 µm, respectively.

loss at 6 to 7 days post-inoculation (Jha et al. 2022, Golden et al. 2020). The high mortality rate within the first week of infection indicates the mice's high susceptibility to SARS-CoV-2, which aligns with previous findings (Dong et al. 2022; Golden et al. 2020). However, treatment with equine-derived hyperimmune serum showed promising outcomes in alleviating clinical symptoms and reducing viral load in the lungs and
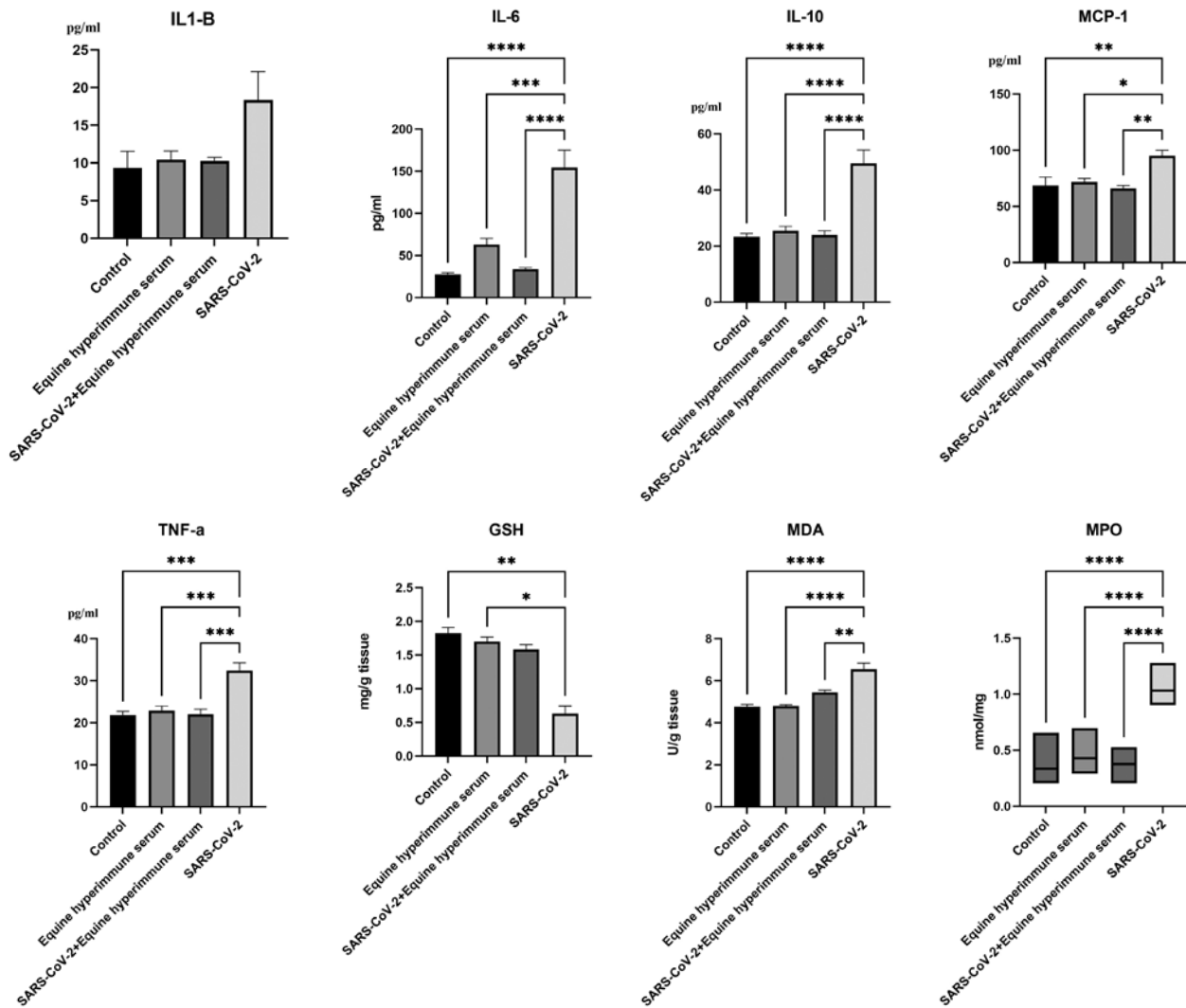
Fig. 8. Oxidative stress parameter analyses of lung tissues (GSH, MDA and, MPO) and serum cytokine levels (IL 1-B, IL 6, IL 10, MCP-1 and, TNF-α) were measured in K18 hACE2 transgenic mice 4 to 14 days after being exposed to SARS-CoV-2. (* p<0.05, ** p<0.01, *** p<0.001, **** p<0.0001)

heart, with complete resolution observed by the 14th day of observation.

Viral load quantification from tissue samples revealed that the lungs were the most significantly affected organs in terms of viral accumulation, with the heart also showing statistically significant viral load compared to the negative control group. However, treatment with hyperimmune serum resulted in significantly lower viral RNA load in both the lungs and heart, indicating that the hyperimmune serum may have a neutralizing effect on the virus and reduce its replication in these organs. This is consistent with previous studies that have shown the potential of equine-derived hyperimmune serum in neutralizing SARS-CoV-2 in vitro (Jha et al. 2022).

Histopathological examination of the nasal passages and lungs further supported the beneficial effects of hyperimmune serum treatment. In the SARS-CoV-2 infected group, severe damage to the olfactory epithelium, inflammatory cell infiltration, and accumulation of mucus were observed in the nasal passages. In contrast, the group treated with hyperimmune serum showed only mild inflammation and mild epithelial lesions, indicating that hyperimmune serum may have a protective effect on the nasal passages. Similarly, in the lungs, the SARS-CoV-2 group showed interstitial pneumonia, capillary congestion, and thickening of the alveolar septum, while the equine hyperimmune serum-treated infection group showed mild infection with mostly preserved alveolar airspaces.

Further analysis of lung tissue samples revealed reduced oxidative stress in the group administered with serum, likely attributable to diminished infection. Moreover, assessment of pro-inflammatory cytokines in the serum revealed significant differences in the levels of IL-10, MCP-1, and TNF-α in the serum-treated

group. Remarkably, these cytokines are frequently associated with the severity of COVID-19 in the literature (Golden et al. 2020). The decreased levels of these cytokines suggest that the serum treatment may potentially ameliorate cytokine storm, a prominent complication of COVID-19.

To avoid the risk of antibody-dependent enhancement (ADE) of infection, pooled plasma obtained from all four horses 48 days after the first immunization was processed to remove the Fc portion of IgG by pepsin digestion, followed by partial purification of the F(ab')2 fragment by ammonium sulfate fractionation (Pan et al. 2020).

Our study supports prior research on equine-derived hyperimmune serum as a potential treatment for reducing viral load and alleviating clinical symptoms (Luis Eduardo Cunha et al. 2020, Pan et al. 2020, León et al. 2021, Moreira-Soto et al. 2021). Hyperimmune serum improved outcomes, reduced viral replication, and decreased inflammation. It may be a viable option for early-stage pandemic passive immunotherapy.

The novelty of this study is the use of the whole virus and ALUM gel adjuvant, which has been shown to enhance the immune response and have a longer-lasting effect on immunity, while causing fewer localized reactions in horses compared to Freund's adjuvant. This is important from an animal welfare perspective and may make ALUM gel a preferred adjuvant for hyperimmunization in horses. Sequencing of the complete genome of the virus strain used for inactivated antigen production was done to avoid significant mutations that may occur, particularly in the RBD region. This ensures that the hyperimmune serum generated in this study is specifically targeted against the circulating strain of SARS-CoV-2 in Turkey, increasing its potential effectiveness. Also in this study, we aimed to achieve high antibody titers and minimal systemic effects using the SARS-CoV-2 strain that yielded high antibody levels in previous SARS-CoV-2 vaccine studies. The inactivated SARS-CoV-2 was purified by multimodal chromatography (size exclusion and ion exchange) to be optimally free from all medium and host cell residues. The antigen was absorbed over 98% with ALUM gel." and "Sequencing of the complete genome of the virus strain used for inactivated antigen production was done to avoid significant mutations that may occur, particularly in the RBD region. This ensures that the hyperimmune serum generated in this study is specifically targeted against the circulating strain of SARS-CoV-2 in Turkey, increasing its potential effectiveness."

In conclusion, our study demonstrates the potential of equine-derived hyperimmune serum as a viable option for passive immunotherapy in the early stages of a pandemic when specific treatments are not yet available. The use of ALUM gel adjuvant and the inclusion of the circulating strain of SARS-CoV-2 in Turkey in the antigen preparation are notable strengths of our study. With standardized guidelines from the WHO, equine antibody products may be readily available worldwide, providing an additional tool in the fight against emerging viral pathogens such as SARS-CoV-2.

Acknowledgements

References

Botosso VF, Jorge SAC, Astray RM, Guimaraes AMS, Mathor MB, Carneiro PS, Durigon EL, Covas D, Oliveira DBL, Oliveira RN, Maria DA, Eto SF, Gallina NMF, Pidde G, Squaiella-Baptistão CS, Silva DT, Villas-Boas IM, Fernandes DC, Auada AVV, Banari AC, Filho AFS, Bianconi C, Utescher CLA, Oliveira DCA, Mariano DOC, Barbosa FF, Rondon G, Kapronezai J, Silva J G, Goldfeder MB, Comone P, Junior REC, Pereira TTS, Wen FH, Tambourgi DV, Chudzinski-Tavassi AM **(2022)** Anti-SARS-CoV-2 equine F (Ab′)2 immunoglobulin as a possible therapy for COVID-19. Sci Rep 12: 3890.

De Vito A, Colpani A, Saderi L, Puci M, Zauli B, Fiore V, Fois M, Meloni MC, Bitti A, Di Castri C, Maida I, Babudieri S, Sotgiu G, Madeddu G. **(2022)** Impact of early SARS-CoV-2 antiviral therapy on disease progression. Viruses 15: 71.

Dong W, Mead H, Tian L, Park JG, Garcia JI, Jaramillo S, Barr T, Kollath DS, Coyne VK, Stone NE, Jones A, Zhang J, Li A, Wang LS, Milanes-Yearsley M, Torrelles JB, Martinez-Sobrido L, Keim PS, Barker BM, Caligiuri MA, Yu J **(2022)** The K18-Human ACE2 transgenic mouse model recapitulates non-severe and severe COVID-19 in response to an infectious dose of the SARS-CoV-2 virus. J Virol: e0096421.

Golden JW, Cline CR, Zeng X, Garrison AR, Carey BD, Mucker EM, White LE, Shamblin JD, Brocato RL, Liu J, Babka AM, Rauch HB, Smith JM, Hollidge BS, Fitzpatrick C, Badger CV, Hooper JW **(2020)** Human angiotensin-converting enzyme 2 transgenic mice infected with SARS-CoV-2 develop severe and fatal respiratory disease. JCI Insight 5: e142032.

Jha A, Barker D, Lew J, Manoharan V, Kessel JV, Haupt R, Toth D, Frieman M, Falzarano D, Kodihalli S **(2022)** Efficacy of COVID-HIGIV in animal models of SARS-CoV-2 infection. Sci Rep 12: 16956.

León G, Herrera M, Vargas M, Arguedas M, Sánchez A, Segura A, Gómez A, Solano G, Aguilar E C, Risner K,

Narayanan A, Bailey C, Villalta M, Hernández A, Sánchez A, Cordero D, Solano D, Durán G, Segura E, Cerdas M, Umaña D, Moscoso E, Estrada R, Gutiérrez J, Méndez M, Castillo AC, Sánchez L, Sánchez R, Gutiérrez JM, Díaz C, Alape A **(2021)** Development and characterization of two equine formulations towards SARS-CoV-2 proteins for the potential treatment of COVID-19. Sci Rep 11: 9825.

Li E, Han Q, Bi J, Wei S, Wang S, Zhang Y, Liu J, Feng N, Wang T, Wu J, Yang S, Zhao Y, Liu B, Yan F, Xia X **(2023)** Therapeutic equine hyperimmune antibodies with high and broad-spectrum neutralizing activity protect rodents against SARS-CoV-2 infection. Front Immunol 14: 1066730.

Luis Eduardo Cunha, Stolet AA, Strauch MA, Pereira VAR, Dumard CH, Gomes AMO, Souza PNC, Fonseca JG, Pontes FE, Meirelles LGR, Albuquerque JWM, Sacramento CQ, Rodrigues NF, Lima TM, Alvim RGF, Marsili FF, Caldeira MM, Higa LM, Monteiro FL, Zingali RB, Oliveira GAP, Souza TML, Tanuri A, Oliveira AC, Guedes H L M, Castilho L R , Silva J L **(2020)** Potent neutralizing equine antibodies raised against recombinant SARS-CoV-2 spike protein for COVID-19 passive immunization therapy. Cold Spring Harbor Laboratory, bioRxiv 17: 254375

Maccio U, Zinkernagel AS, Shambat SM, Zeng X, Cathomas G, Ruschitzka F, Schuepbach RA, Moch H, Varga Z. SARS-CoV-2 **(2021)** Leads to a small vessel endotheliitis in the heart. EBioMedicine 63: 103182.

Moreira-Soto A, Arguedas M, Brenes H, Buján W, Corrales--Aguilar E, Díaz C, Echeverri A, Flores-Díaz M, Gómez A, Hernández A, Herrera M, León G, Macaya R, Kühne A, Molina-Mora JA, Mora J, Sanabria A, Sánchez A, Sánchez L, Segura Á, Segura E, Solano D, Soto C, Stynoski JL, Vargas M, Villalta M, Reusken CBEM, Drosten C, Gutiérrez JM, Alape-Girón A, Drexler JF **(2021)** High efficacy of therapeutic equine hyperimmune antibodies against SARS-CoV-2 variants of concern. Frontiers in Medicine. 8: 735853.

Onen EA, Sonmez K, Yildirim F, Demirci EK, Gurel A **(2022)** Development, analysis, and preclinical evaluation of inactivated vaccine candidate for prevention of Covid-19 disease. All Life 15: 771-793.

Pan X, Zhou P, Fan T, Wu Y, Zhang J, Shi X, Shang W, Fang L, Jiang X, Shi J, Sun Y, Zhao S, Gong R, Chen Z, Xiao G **(2020)** Immunoglobulin fragment F(ab')2 against RBD potently neutralizes SARS-CoV-2 in vitro. Antiviral Res 182: 104868.

Schoell A, Heyde B, Weir D, Po-Chang C, Yiding H, Tung D **(2009)** Euthanasia method for mice in rapid time-course pulmonary. Pharmacokinetic Studies 48: 506.

Suvarna KS, Layton C, Bancroft JD **(2018)** Bancroft's theory and practice of histological techniques E-Book. Elsevier health sciences, Philadelphia, pp 286-291.

Winkler ES, Bailey AL, Kafai NM, Nair S, McCune BT, Yu J, Fox JM, Chen RE, Earnest JT, Keeler SP, Ritter JH, Kang L, Dort S, Robichaud A, Head R, Holtzman MJ, Diamond MS **(2020)** SARS-CoV-2 infection of human ACE2-transgenic mice causes severe lung inflammation and impaired function. Nat Immunol 21: 1327-1335.

Xu J, Xu X, Jiang L, Dua K, Hansbro PM, Liu G **(2020)** SARS-CoV-2 induces transcriptional signatures in human lung epithelial cells that promote lung fibrosis. Respir Res 21: 182.

Yu P, Deng W, Bao L, Qu Y, Xu Y, Zhao W, Han Y, Qin C **(2022)** Comparative pathology of the nasal epithelium in K18-hACE2 Tg mice, hACE2 Tg mice, and hamsters infected with SARS-CoV-2. Vet Pathol 59: 602-612.

Zhang Q, Wang Y, Qi C, Shen L, Li J **(2020)** Clinical trial analysis of 2019-nCoV therapy registered in China. J Med Virol 92: 540-545.